CHINESE OPTICS LETTERS

Vol. 21, No. 5 | May 2023

Heat accumulation effects in femtosecond laser-induced subwavelength periodic surface structures on silicon

Qiang Fu (付 强)[1,2], Jing Qian (钱 静)[1,2], Guande Wang (王关德)[1,2], and Quanzhong Zhao (赵全忠)[1,2*]

[1] State Key Laboratory of High Field Laser Physics and CAS Center for Excellence in Ultra-intense Laser Science, Shanghai Institute of Optics and Fine Mechanics, Chinese Academy of Sciences, Shanghai 201800, China

[2] University of Chinese Academy of Sciences, Beijing 100049, China

*Corresponding author: zqz@siom.ac.cn

Received December 7, 2022 | Accepted February 8, 2023 | Posted Online May 6, 2023

High-repetition rate femtosecond lasers are shown to drive heat accumulation processes that are attractive for femtosecond laser-induced subwavelength periodic surface structures on silicon. Femtosecond laser micromachining is no longer a nonthermal process, as long as the repetition rate reaches up to 100 kHz due to heat accumulation. Moreover, a higher repetition rate generates much better defined ripple structures on the silicon surface, based on the fact that accumulated heat raises lattice temperature to the melting point of silicon (1687 K), with more intense surface plasmons excited simultaneously. Comparison of the surface morphology on repetition rate and on the overlapping rate confirms that repetition rate and pulse overlapping rate are two competing factors that are responsible for the period of ripple structures. Ripple period drifts longer because of a higher repetition rate due to increasing electron density; however, the period of laser structured surface is significantly reduced with the pulse overlapping rate. The Maxwell–Garnett effect is confirmed to account for the ripple period-decreasing trend with the pulse overlapping rate.

Keywords: laser materials processing; femtosecond laser; subwavelength periodic surface structures.
DOI: 10.3788/COL202321.051402

1. Introduction

Femtosecond laser-induced periodic surface structures (fs-LIPSSs) on various materials, such as metals, semiconductors[1–6], and dielectrics[7], have gained considerable attention and hold many potential applications in enhancing tungsten filament luminous efficiency[8], enhancement of optical absorption and photocurrents[9], metal colorization[10,11], terahertz-emitting enhancement[12], modulation of tribological property[13,14], and superhydrophobic modification[15]. The mechanism responsible for fs-LIPSSs is still a matter of debate. However, it is widely accepted that a low spatial frequency LIPSS (period $> l/2$) is based on the interference of surface plasmons (SPs) and incident lasers[16–18]. It has been shown that the well-shaped periodic structures are created when the laser fluence lies slightly above the damage threshold of materials[19]. The dependence of the surface morphology, such as spatial period, orientation, and depth on laser fluence, pulse overlapping rate, incident angle, laser polarization, pulse duration, and wavelength has been extensively investigated[20]. However, the mechanism of high-repetition LIPSS formation seems to be even more complex and few studies have been reported. High-repetition rate femtosecond laser pulses are shown to drive heat accumulation processes, which are attractive for rapid writing of low-loss optical waveguides in transparent glasses[21]. Unfortunately, the heat accumulation effects on periodic surface structures still remain unclear. In this Letter, variable repetition rates between 10 and 400 kHz were used to study the relationship between heat accumulation and the resultant periodic surface structures on a silicon surface. In addition, writing parameters, such as the pulse overlapping rate, were also varied. In our case, heat accumulation was shown to enhance the formation of LIPSSs not previously recognized, and the Maxwell–Garnett effect was proved to be responsible for the reduced period with the pulse overlapping rate.

2. Experiment

A commercial amplified solid-state ultrashort pulsed laser system (TruMicro 5070 Femtosecond Edition) with 1030 nm wavelength, 900 fs pulse duration, and 400 kHz repetition rate was used as the irradiation source. The beam was first transported by reflective optics, and then was focused on the sample surface by a galvanometer laser scanning system (ScanLab). The beam diameter before focusing was 5 mm and the beam was focused on a spot size of 35 μm in diameter. A silicon sample with ⟨111⟩

facet was mounted on a platform. A fluence of 0.25 J/cm^2 was ensured so that the fluence was near the damage threshold of silicon. The laser polarization was perpendicular to the scanning direction, and the laser was in normal incidence. The morphology of induced structures was examined by scanning electron microscopy (JSM-6360LA).

3. Results and Discussion

With a pulse overlapping rate of 91%, the influence of the repetition rate on surface morphology is shown in Figs. 1(a)–1(e). Figure 1(f) shows the ripple period and the scanning line width as a function of repetition rate. The resultant fringes are in the subwavelength scale, with period increasing from 0.9 to 0.97 μm when repetition rate is varied from 10 to 400 kHz; the subwavelength periodic pattern is rough at a low repetition rate, whereas it is intensively enhanced at a higher repetition rate; with growing repetition rate, the scanning line widens, and the sharp increase is at 100 kHz.

During the laser irradiation, the laser energy is absorbed by free electrons due to the inverse bremsstrahlung. The absorption process is followed by thermalization within the electron subsystem, energy transfer from the electrons to the lattice, and heat transport into the target due to the electron thermal diffusion[22]. The lattice heating time is over a picosecond time scale. According to the numerical investigation of Chen *et al.*, the lattice temperature at heat equilibrium is estimated to be 1000 K. Subsequently, the lattice follows a heat diffusion process[23],

$$c_l \frac{\partial T_l}{\partial t} = k_l \frac{\partial^2 T_l}{\partial z^2},$$
$$\text{with} \quad C_l = 1.978 + 3.54 \times 10^{-4} T_l - 3.68 T_l^{-2} \,[\mathrm{J/(cm^3 \cdot K)}]$$
$$\text{and} \quad k_l = 1585 T_l^{-1.23} \,[\mathrm{W/(cm \cdot K)}], \tag{1}$$

where z is the direction perpendicular to the target surface, T_l, C_l, and k_l are the temperature, heat capacity, and thermal conductivity of the lattice, respectively. The form solution of Eq. (1) is

$$T_l = \sum_{m=1}^{\infty} A_m e^{-a^2 \omega_m^2 t} \sin \omega_m z \tag{2}$$

when the temperature of only the irradiation point is considered. Equation (2) can be simplified as

$$T_l = A e^{-B^2 t} + C \left(B = \omega \sqrt{\frac{k_l}{C_l}} \right), \tag{3}$$

where A is the temperature of the lattice after a single laser pulse irradiation, ω is the spatial frequency of temperature, and C is room temperature. Figure 2(a) depicts the surface temperature decay of the silicon after a single pulse irradiation. It is obvious that the temperature decreases to 517 K at 2.5 μs and 300 K at 100 μs. That is, at a 10-kHz repetition rate, the temperature relaxes to the room temperature (300 K) before the next pulse arrives, which results in no accumulation of heat [Fig. 2(b)], while at a 400-kHz repetition rate, heat accumulation is strongly evident, leading to a growing temperature with increasing pulse numbers [Fig. 2(c)]. Meanwhile, heat accumulation gives rise to a broader ablation area. So we can find in Fig. 1(f) that the scanning line width increases from about 27 to 31 μm, with a repetition rate varying from 10 to 400 kHz.

Morphological characteristics of subwavelength ripple structures induced by femtosecond laser pulses with pulse overlapping rates varying from 65% to 98% are illustrated in Figs. 3(a)–3(e). At a pulse overlapping rate of 65%, ripple structures emanate from a surface scratch denoted in the blue dashed circle [Fig. 3(a)]. The scratch is approximately 1 μm in length. Unlike the observed subwavelength structures in Fig. 1, the

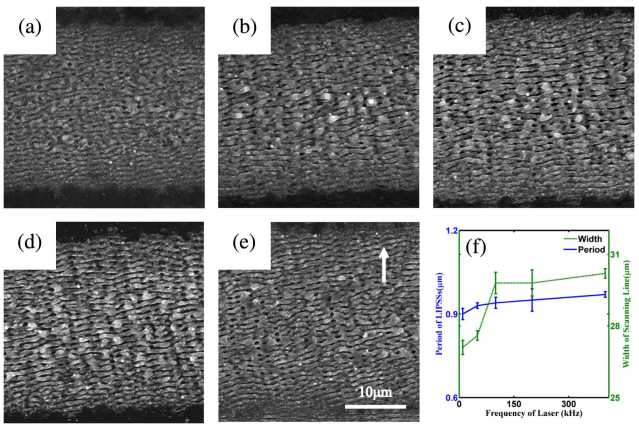

Fig. 1. SEM images of subwavelength ripples induced by femtosecond laser pulses under repetition rates of (a) 10 kHz, (b) 50 kHz, (c) 100 kHz, (d) 200 kHz, and (e) 400 kHz at a pulse overlapping rate of 91%; (f) period of ripples and width of the scanning line as a function of repetition rate (SEM magnification, 2000; scale bar, 10 μm; white arrow, laser polarization).

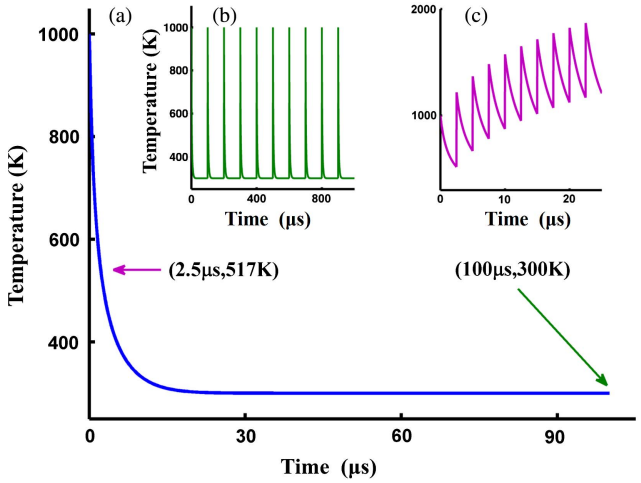

Fig. 2. (a) Surface temperature decay of silicon after a single pulse irradiation; calculated temperature as a function of time for repetition rates of (b) 10 kHz and (c) 400 kHz, respectively.

period of the cone-shaped fringes in this case is as long as the wavelength of the incident laser. A model of nonradiative "radiation remnants" can be responsible for the observed phenomenon, based on the assumption that the steady-state patterns result from inhomogeneous energy absorption just beneath the surface, induced by surface roughness[24,25]. When the pulse overlapping rate is increased to 83%, subwavelength periodic structures can not only be observed in the central area of the laser ablation region, but also begin to appear in the periphery area. We also note that the subwavelength ripple goes with a shorter period and deeper grooves in the periphery (marked by a red ellipse) [Fig. 3(b)]. In Fig. 3(f), it is evident that the ripple period becomes shorter with increased pulse overlapping rate. In addition, the repetition rate of 400 kHz induces a longer ripple period than that of 100 kHz at the same pulse overlapping rate.

The subwavelength surface ripples are considered to be due to SP–laser interference[20]. The propagating SPs and the incident laser interfere to form a fringe with a period written as

$$\Lambda = \frac{\lambda}{\left(\frac{\lambda}{\lambda_{sp}} + \sin\theta\right)}, \tag{4}$$

where Λ is the ripple period, λ is the laser wavelength, and θ is the beam incident angle. λ_{sp} is the wavelength of SPs and is given by

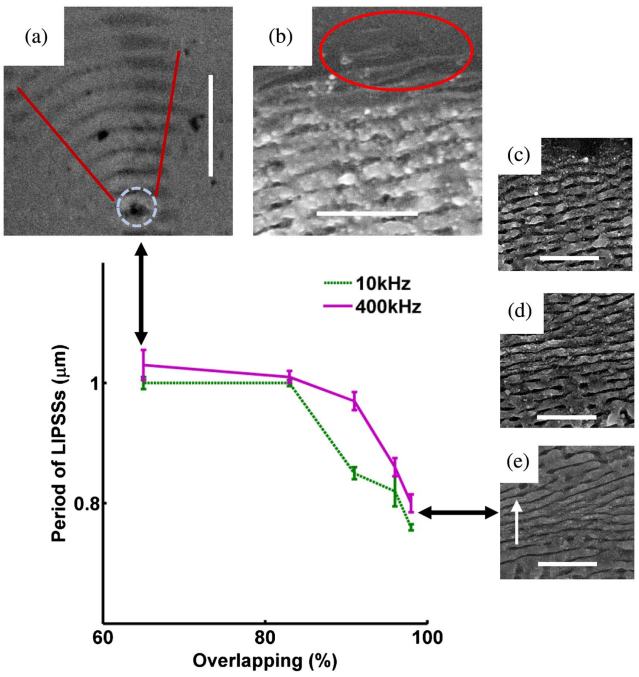

Fig. 3. SEM images of ripple structures induced by femtosecond laser pulses under pulse overlapping rates of (a) 65%, (b) 83%, (c) 91%, (d) 96%, and (e) 98% at a repetition rate of 400 kHz; (f) period of ripples as a function of the pulse overlapping rate at repetition rates of 10 and 400 kHz (SEM magnification, 3500; scale bar, 5 μm; white arrow, laser polarization).

$$\lambda_{sp} = \left(\frac{\lambda}{\sqrt{\varepsilon_1}}\right)\sqrt{\frac{1}{\varepsilon_1} + \frac{1}{\varepsilon'(\omega)}}, \tag{5}$$

where ε_1 is the dielectric constant of the substance above the air–silicon interface, and $\varepsilon'(\omega)$ is the real part of the dielectric constant of the highly excited silicon surface. In normal incidence ($\theta = 0°$), we obtain the simple relationship $\Lambda = \lambda_{sp}$. Owing to the laser-induced plasma, $\varepsilon'(\omega)$ can be described with the Drude model,

$$\varepsilon'(\omega) = \varepsilon_c - \frac{\omega_p^2}{(\omega^2 + \gamma^2)}, \tag{6}$$

where ε_c is the dielectric constant of the silicon surface in a normal state (without laser-induced free electrons) and $\gamma = 1/\tau$ is the electron collision frequency. $\varepsilon'(\omega)$ has been proved to fulfill the metallic condition $\varepsilon'(\omega) < -1$, for both dielectrics and semiconductors[26,27]. Therefore, we can deduce from Eq. (5) that λ_{sp} is always smaller than λ, which agrees with the experimental observations in our case and is precisely the origin of the subwavelength characteristic of such ripples. ω_p is the plasma frequency,

$$\omega_p = \sqrt{\frac{N_e q^2}{m_e \varepsilon_0}}, \tag{7}$$

where q is the electric charge and m_e is the electron effective mass. N_e is the electron density, and follows a Boltzman distribution with electron temperature (T),

$$N_e = 2\left(\frac{m_e k_B T}{2\pi\hbar}\right)^{3/2} F_\xi(\eta_e), \tag{8}$$

where $F_\xi(\eta_e)$ is the ξ-fold Fermi–Dirac integral.

We estimated that substance above the air–silicon interface is air ($\varepsilon_1 \approx 1$), so the ripple period is simplified as

$$\Lambda = \lambda_{sp} = \lambda\sqrt{1 + \frac{1}{\varepsilon'(\omega)}}. \tag{9}$$

Increasing laser pulse irradiation gives rise to a higher lattice and electron temperature and therefore higher N_e. For $\varepsilon'(\omega) < -1$, with increasing N_e, $|\varepsilon'(\omega)|$ increases; thus, from Eq. (9), Λ increases. This Λ-increasing trend with growing temperature agrees well with observations in Fig. 1, where Λ lengthens with increasing repetition rates, and in Fig. 3(f), where the repetition rate of 400 kHz results in a longer ripple period than that of 100 kHz. As described above, the ripple period in the periphery becomes shorter with deepened grooves [Fig. 3(b)]. This effect can be accounted for by the Gaussian distribution of the laser fields, where fluence in the periphery is much lower. Accordingly, by Eq. (9), lower periphery fluence means lower periphery N_e, and therefore gives rise to shorter Λ.

Huang *et al.* proposed that period-decreasing with increasing pulse overlapping rate is due to grating-assisted SP–laser

coupling[20]. When the initial ripples are formed, deeper grooves make the laser field transfer to SPs more efficiently because of grating coupling effects. Hence, grooves grow as the number of pulses increases. As the groove deepens, the ripple period should decrease in order to satisfy the grating coupling condition. Based on this model, they also put forward an exceptional situation. When heat accumulation exists, a strong thermal effect will induce a thick melted layer and baffle the deepening of the groove. Accordingly, the grating coupling effect is weak, and the value of Λ is mainly due to the interference mechanism and remains almost constant near λ as the pulse number increases.

However, in Fig. 3(f), it is evident that even at a repetition rate of 400 kHz where heat accumulation is quite strong, the ripple period still obeys an obvious decay trend with an increasing pulse overlapping rate. Therefore, we propose that the origin of the significantly reduced period with growing pulse overlapping rate is actually due to the Maxwell–Garnett effect[28]. During laser irradiation, the silicon surface was covered by extensive nanostructures. The femtosecond laser structured surface can be divided into two layers: a uniform LIPSS layer and an air–nanostructure composite layer. In this case, ε_1 cannot be estimated to be 1 but should be replaced by the effective dielectric constant (ε_{eff} of the air–nanostructure composite). Therefore, ε_{eff} is estimated using the Maxwell–Garnett theory[26],

$$\varepsilon_{\text{eff}} = \varepsilon_1 \frac{\varepsilon' + 2\varepsilon_1 + 2f(\varepsilon' - \varepsilon_1)}{\varepsilon' + 2\varepsilon_1 - f(\varepsilon' - \varepsilon_1)}, \tag{10}$$

where f is the volume fraction of the silicon inclusion in air–nanostructure composite. So λ_{sp} should be rewritten as

$$\Lambda = \lambda_{\text{sp}} = \left(\frac{\lambda}{\sqrt{\varepsilon_{\text{eff}}}}\right)\sqrt{\frac{1}{\varepsilon_{\text{eff}}} + \frac{1}{\varepsilon'}}. \tag{11}$$

Based on Eq. (9), we calculate and plot the λ_{sp} as a function of N_e [Fig. 4(a)]. As discussed above, λ_{sp} increases with growing N_e. The effective dielectric constant of the air–nanostructure composite (ε_{eff}) and SP wavelength (λ_{sp}) as functions of volume fraction of the silicon inclusion (f) are plotted in Fig. 4(b). With an increasing pulse overlapping rate, more nanostructures are generated, and f is therefore strongly enhanced. We notice that ε_{eff} continuously increases with f. This increase in ε_{eff} eventually reduces λ_{sp}.

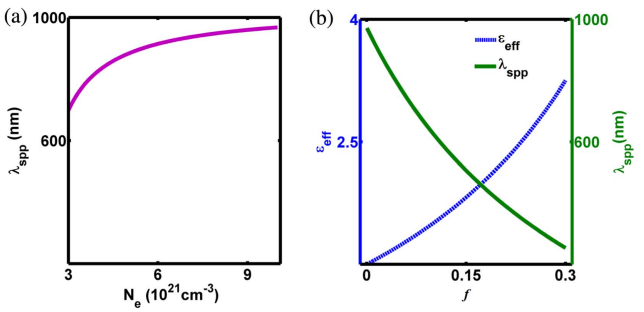

Fig. 4. (a) SP wavelength as a function of electron density; (b) effective dielectric constant (ε_{eff}) of air–nanostructure composite on LIPSSs and SP wavelength as functions of volume fraction of the silicon inclusion.

Therefore, we can conclude that both the electron density and the volume fraction of the silicon inclusion are responsible for λ_{sp}. In the formation of LIPSSs, the increasing pulse overlapping rate propels both the electron density and the volume fraction of the silicon inclusion to go up. However, higher electron density drifts λ_{sp} toward longer, whereas increasing volume fraction drives λ_{sp} toward shorter. The two mechanisms compete with each other. Finally, in our case, the volume fraction of the silicon inclusion plays a more important role, which agrees with our observations in Fig. 3(f). That is, Λ is significantly reduced with the increasing pulse overlapping rate, whereas Λ at a repetition rate of 400 kHz is slightly more enhanced than that at a repetition rate of 10 kHz. Moreover, the weak dependence of Λ on repetition rates can also be observed in Fig. 1(f): Λ exhibits a small increase from 0.9 to 0.97 μm when the repetition rate is varied from 10 to 400 kHz.

In addition, surface morphology under repetition rates of 10 and 400 kHz is compared. Figures 5(a)–5(c) are the LIPSSs under a repetition rate of 10 kHz, and Figs. 5(d)–5(f) are under 400 kHz. We can find that LIPSSs in Figs. 5(a)–5(c) are attached by micro- or nanoparticles, and therefore look somewhat obscure. In contrast, the repetition rate of 400 kHz produces more distinct and defined ripples. It is due to heat accumulation that lattice temperature is well above the melting point of silicon (1687 K) and more intense SPs are stimulated. The molten silicon is forced into periodic distribution by the high pressure of stimulated SPs. Once the lattice temperature relaxes, periodic distribution is solidified into periodic structures. The more intense the stimulated SPs are, the more regularly and tidily the silicon surface is engraved. So, in Figs. 1(a)–1(e), LIPSSs become more evident and neat with growing repetition rates.

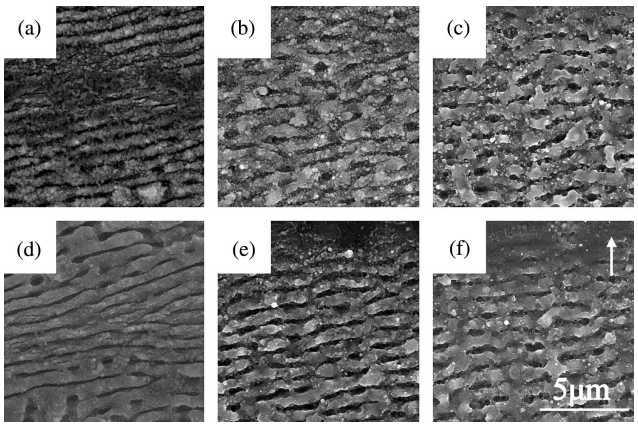

Fig. 5. Comparison of the surface morphology under (a)–(c) 10 kHz and (d)–(f) 400 kHz at pulse overlapping rates of (a), (d) 98%, (b), (e) 91%, and (c), (f) 83%, respectively (SEM magnification, 3500; scale bar, 5 μm; white arrow, laser polarization).

4. Conclusion

In conclusion, variable repetition rates between 10 and 400 kHz were used to study the relationship between heat accumulation and resulting periodic surface structures on silicon. It was found that when the repetition rate reached up to 100 kHz, heat accumulation became so evident that femtosecond laser micromachining could not be considered as a nonthermal process. Moreover, heat accumulation was shown to significantly enhance LIPSSs, which has not been previously recognized. The ripple morphology under higher repetition appeared more distinct and much neater as more intense SPs were stimulated, and accumulated heat gave rise to a molten silicon surface. Once the temperature relaxes, SP-induced periodic distribution on the silicon surface is solidified into periodic structures. The more intense the stimulated SPs are, the much better-defined and neater ripples are engraved on the silicon surface. In addition, the ripple period was confirmed to be accounted for by two competing factors: repetition rate and pulse overlapping rate. The ripple period drifted longer with a higher repetition rate, whereas it was significantly reduced by increasing the pulse overlapping rate. The increase in period with repetition rates is due to increased electron density. However, ripple period-decreasing trend with a growing pulse overlapping rate is proposed to be due to the volume fraction increase of the silicon inclusion in the air–nanostructure composite, based on the Maxwell–Garnett theory.

Acknowledgement

This work was supported by the National Natural Science Foundation of China (Nos. 52175377 and 12174411).

References

1. J. Reif, O. Varlamova, M. Ratzke, M. Schade, H. S. Leipner, and T. Arguirov, "Multipulse feedback in self-organized ripples formation upon femtosecond laser ablation from silicon," Appl. Phys. A **101**, 361 (2010).
2. E. Allahyari, J. J. Nivas, M. Valadan, R. Fittipaldi, A. Vecchione, L. Parlato, R. Bruzzese, C. Altucci, and S. Amoruso, "Plume shielding effects in ultrafast laser surface texturing of silicon at high repetition rate in air," Appl. Surf. Sci. **488**, 128 (2019).
3. J. J. Nivas and S. Amoruso, "Generation of supra-wavelength grooves in femtosecond laser surface structuring of silicon," Nanomaterials **11**, 174 (2021).
4. X. Jia, Y. Yuan, D. Yang, T. Jia, and Z. Sun, "Ultrafast time-resolved imaging of femtosecond laser-induced periodic surface structures on GaAs," Chin. Opt. Lett. **12**, 113203 (2014).
5. K. Cao, L. Chen, K. Cheng, Z. Sun, and T. Jia, "Regular uniform large-area subwavelength nanogratings fabricated by the interference of two femtosecond laser beams via cylindrical lens," Chin. Opt. Lett. **18**, 093201 (2020).
6. M. Hu, J. J. Nivas, M. Valadan, R. Fittipaldi, A. Vecchione, R. Bruzzese, C. Altucci, and S. Amoruso, "Ultrafast laser surface irradiation of silicon: effects of repetition rate in vacuum and air," Appl. Surf. Sci. **606**, 154869 (2022).
7. Y. Yuan and J. Chen, "Grating-assisted fabrication of sub-wavelength ripples during femtosecond laser processing of dielectrics," Chin. Opt. Lett. **14**, 011404 (2016).
8. A. Y. Vorobyev, V. S. Makin, and C. Guo, "Brighter light sources from black metal: significant increase in emission efficiency of incandescent light sources," Phys. Rev. Lett. **102**, 234301 (2009).
9. Q. Z. Zhao, F. Ciobanu, S. Malzer, and L. J. Wang, "Enhancement of optical absorption and photocurrent of 6 H-SiC by laser surface nanostructuring," Appl. Phys. Lett. **91**, 121107 (2007).
10. A. Y. Vorobyev and C. Guo, "Colorizing metals with femtosecond laser pulses," Appl. Phys. Lett. **92**, 041914 (2008).
11. Y. Li, J. Qian, F. Bai, Z. Wang, C. Wang, W. Fan, Y. Zhang, and Q. Zhao, "Azimuthal angle-and scanning pitch-dependent colorization of metals by ultrashort laser pulses," Appl. Phys. A **122**, 282 (2016).
12. J. Madéo, A. Margiolakis, Z. Y. Zhao, P. J. Hale, M. K. Man, Q. Z. Zhao, W. Peng, W. Z. Shi, and K. M. Dani, "Ultrafast properties of femtosecond-laser-ablated GaAs and its application to terahertz optoelectronics," Opt. Lett. **40**, 3388 (2015).
13. C. Y. Chen, B. H. Wu, C. J. Chung, W. L. Li, C. W. Chien, P. H. Wu, and C. W. Cheng, "Low-friction characteristics of nanostructured surfaces on silicon carbide for water-lubricated seals," Tribol. Lett. **51**, 127 (2013).
14. Z. Wang, Q. Zhao, and C. Wang, "Reduction of friction of metals using laser-induced periodic surface nanostructures," Micromachines **6**, 1606 (2015).
15. V. Zorba, E. Stratakis, M. Barberoglou, E. Spanakis, P. Tzanetakis, S. H. Anastasiadis, and C. Fotakis, "Biomimetic artificial surfaces quantitatively reproduce the water repellency of a lotus leaf," Adv. Mater. **20**, 4049 (2008).
16. S. Brueck and D. Ehrlich, "Stimulated surface-plasma-wave scattering and growth of a periodic structure in laser-photodeposited metal films," Phys. Rev. Lett. **48**, 1678 (1982).
17. V. Schmidt, W. Husinsky, and G. Betz, "Dynamics of laser desorption and ablation of metals at the threshold on the femtosecond time scale," Phys. Rev. Lett. **85**, 3516 (2000).
18. W. L. Barnes, A. Dereux, and T. W. Ebbesen, "Surface plasmon subwavelength optics," Nature **424**, 824 (2003).
19. Q. Z. Zhao, S. Malzer, and L. J. Wang, "Formation of subwavelength periodic structures on tungsten induced by ultrashort laser pulses," Opt. Lett. **32**, 1932 (2007).
20. M. Huang, F. Zhao, Y. Cheng, N. Xu, and Z. Xu, "Origin of laser-induced near-subwavelength ripples: interference between surface plasmons and incident laser," ACS Nano **3**, 4062 (2009).
21. S. M. Eaton, H. Zhang, P. R. Herman, F. Yoshino, L. Shah, J. Bovatsek, and A. Y. Arai, "Heat accumulation effects in femtosecond laser-written waveguides with variable repetition rate," Opt. Express **13**, 4708 (2005).
22. C. Momma, S. Nolte, B. N. Chichkov, F. V. Alvensleben, and A. Tünnermann, "Precise laser ablation with ultrashort pulses," Appl. Surf. Sci. **109**, 15 (1997).
23. J. K. Chen, D. Y. Tzou, and J. E. Beraun, "Numerical investigation of ultrashort laser damage in semiconductors," Int. J. Heat Mass Transfer **48**, 501 (2005).
24. J. E. Sipe, J. F. Young, J. S. Preston, and H. M. Van Driel, "Laser-induced periodic surface structure. I. Theory," Phys. Rev. B **27**, 1141 (1983).
25. J. F. Young, J. S. Preston, H. M. Van Driel, and J. E. Sipe, "Laser-induced periodic surface structure. II. Experiments on Ge, Si, Al, and brass," Phys. Rev. B **27**, 1155 (1983).
26. M. Huang, F. Zhao, Y. Cheng, N. Xu, and Z. Xu, "Mechanisms of ultrafast laser-induced deep-subwavelength gratings on graphite and diamond," Phys. Rev. B **79**, 125436 (2009).
27. A. J. Pedraza, Y. F. Guan, J. D. Fowlkes, and D. A. Smith, "Nanostructures produced by ultraviolet laser irradiation of silicon. I. Rippled structures," J. Vac. Sci. Technol. **22**, 2823 (2004).
28. T. Y. Hwang and C. Guo, "Angular effects of nanostructure-covered femtosecond laser induced periodic surface structures on metals," J. Appl. Phys. **108**, 073523 (2010).